How Do Differences in Electronic Structure Affect the Use of Vanadium Intermediates as Mimics in Non-heme Iron Hydroxylases?

Vyshnavi Vennelakanti[1,2], Mugyeom Jeon[1,2], and Heather J. Kulik[1,2,*]

[1]*Department of Chemical Engineering, Massachusetts Institute of Technology, Cambridge, MA 02139, USA*

[2]*Department of Chemistry, Massachusetts Institute of Technology, Cambridge, MA 02139, USA*

*corresponding author email: hjkulik@mit.edu

ABSTRACT: Vanadyl species are frequently employed as structural mimics of the fleeting Fe(IV)=O intermediate in C–H hydroxylation carried out by non-heme iron hydroxylases. We study active site models of non-heme iron hydroxylases and their vanadium-based mimics using density functional theory to determine if vanadyl is a faithful structural mimic. We identify crucial structural and energetic differences between ferryl and vanadyl isomers owing to the differences in their ground electronic states, i.e., high-spin (HS) for Fe and low-spin (LS) for V. For the succinate cofactor bound to the ferryl intermediate, we predict facile interconversion between monodentate and bidentate coordination isomers for ferryl species but difficult rearrangement for vanadyl mimics. We study isomerization of the oxo intermediate between axial and equatorial positions and find the ferryl potential energy surface to be characterized by a large barrier of ca. 10 kcal/mol that is completely absent for the vanadyl mimic. This analysis reveals even starker contrasts between Fe and V in hydroxylases than have been observed for this metal substitution in non-heme halogenases. Analysis of the relative bond strengths of coordinating carboxylate ligands for Fe and V reveals that all the ligands show stronger binding to V than Fe owing to the LS ground state of V in contrast to the HS ground state of Fe. Overall, the differences in structures, isomer energies, and isomerization energy landscapes between Fe and V highlight the limitations of vanadyl mimics of native non-heme iron hydroxylases.

1. Introduction.

Metalloenzymes catalyze difficult reactions with exquisite selectivity that make their study of interest both for understanding their biological function and for synthetic catalyst design. Exemplary of this are the α-ketoglutarate (αKG)-dependent non-heme iron enzymes[1-3], which carry out C–H activation reactions selectively. C–H activation is difficult to achieve synthetically[4,5] owing to the high C–H bond dissociation energy and its inertness due to low polarity[6]. These non-heme iron enzymes are studied widely[7] and are known to catalyze a variety of reactions such as C–H hydroxylation,[8-12] halogenation,[13-17] epoxidation,[18-21] desaturation,[22] and ring cleavage[23,24]. These reactions play important roles in several biosynthetic processes[25-28] such as primary and secondary metabolism in plants[29], generation of clinically relevant natural products[30-33], DNA repair[34-38] and transcription.[39-41]

Non-heme iron enzymes are also highly selective in nature. For example, non-heme iron halogenases selectively halogenate the substrate even though they also have the potential to carry out hydroxylation.[42] Prior experimental studies supported with computations suggested that substrate positioning[43] and reactivity of the rebound intermediate[44,45] could explain the observed selectivity. Furthermore, computational studies have rationalized the selectivity of these enzymes through various hypotheses including substrate positioning[46,47] using spectroscopic indicators derived from hyperfine sublevel correlation (HYSCORE) spectroscopy,[48-50] isomerization of metal-oxo/hydroxo intermediates,[51,52] interactions with the second coordination sphere,[53] frontier molecular orbital energetics,[54] and OH trapping either through protonation of hydroxo[55] or bicarbonate formation.[56] A recent computational study[57] further demonstrated that the selectivity of halogenases depends on the nature of the substrate radical, with halogen transfer favored for secondary carbon radicals and hydroxo transfer preferred for tertiary carbon radicals. Besides their

selectivity, likely rate-determining aspects of the catalytic cycles of non-heme enzymes including oxygen activation[58-60] and hydrogen atom transfer (HAT)[61-63] have also been computationally investigated.

The most common type of reaction carried out by non-heme iron enzymes is C–H hydroxylation,[29] which is crucial in lipid metabolism[64,65] and biosynthesis of antibiotics such as vancomycin,[66] fosfomycin,[67] and carbapenem.[68] The active site of the αKG-dependent non-heme iron hydroxylases[69,70] consists of the canonical 2-His-1-carboxylate facial triad[14,71,72] bound to an Fe center where the carboxylate is usually Glu/Asp. Ferryl intermediates formed during the catalytic cycle of these enzymes are highly reactive,[9,33,42,73-75] which makes them hard to characterize by experimental techniques[76,77] such as crystallography[78,79] and spectroscopy.[80-83] An experimental approach to structurally characterize these fleeting ferryl intermediates[74] frequently invoked in C–H activation[73,84] is to replace them with more inert V-based mimics, which has been carried out for non-heme iron oxygenases[73,84-86] and hydroxylases.[87] Furthermore, study of vanadyl mimics has been carried out in combination with the spectroscopic guidance derived from HYSCORE spectroscopy.[73] However, this approach is not without limitations, as demonstrated in a prior computational study of vanadyl mimics of non-heme iron halogenases.[88] Given the differences in the electronic structures of Fe and V, and the bond lengths of Fe–His and V–His bonds in the active site intermediates,[88] computational studies are necessary to provide insights into shortcomings of using vanadyl mimics to study ferryl intermediates.

One challenge for the validity of V-based mimics is that C–H hydroxylation carried out by non-heme iron hydroxylases exhibits spin-state dependent reactivity[81,89-97], i.e., non-heme iron enzymes are known to react in the high-spin ground state.[9,49,75,98,99] The electronic structures of Fe(IV)[47,52,55,75,76] and V(IV)[100] in the key metal-oxo intermediate are different, i.e., Fe(IV) and

V(IV) have d^4 and d^1 electronic configurations, respectively. This results in different accessible spin states for Fe(IV)=O and V(IV)=O intermediates, where ferryl intermediates can access three spin states, i.e., high-spin (HS), intermediate-spin (IS), and low-spin (LS), while vanadyl intermediate can only access the LS state. Differences in spin states are also observed for other intermediates along the catalytic cycle, with Fe intermediates accessing all three spin states while V-based mimics are limited to either the LS, or IS and LS states.[88] While it is unknown whether the spin would be conserved across hydroxylation intermediates in a vanadium-containing enzyme, a prior computational study of halogenases[88] showed that the ground spin states of vanadium active sites vary across intermediates.

Previously,[88] we studied whether vanadium-based intermediates are faithful mimics of native non-heme iron halogenases and found differences between non-heme iron halogenase active site structures and those of their vanadium-based mimics. In this study, we compare native ferryl species and their vanadyl mimics for the related non-heme iron hydroxylases. We highlight the limits of using vanadyl mimics for the fleeting ferryl intermediates in C–H hydroxylation through an extensive computational study of isomer structures and energetics in hydroxylases and find even starker differences between Fe and V active site models than for halogenases. While the isomerization energy landscape of V(IV)=O is barrierless in our models, we observe a barrier for isomerization of Fe(IV)=O in hydroxylases that is higher than that observed in non-heme iron halogenases. Additionally, the hydroxylase active site isomerization barrier for structures with monodentate Glu is lower relative to bidentate Glu isomers. This suggests that targeted modifications to the enzyme active site to favor monodentate Glu, e.g., through noncovalent interactions, could preferentially lower the isomerization barrier in engineered hydroxylases. Further examination of ligand binding strengths, i.e., of succinate/Glu/αKG to Fe and V, reveals

that the bidentate αKG binds more strongly to both metals in hydroxylases relative to the equivalent binding in halogenases.

2. Computational Details.

The active sites of a representative non-heme iron hydroxylase, VioC[10,85,101,102] (PDBID: 6ALM) and its vanadyl mimic[87] (PDBID: 6ALR), were extracted from crystal structures of the enzyme. The native active site model comprised the Fe metal center, αKG, two metal-bound His ligands and one metal-bound Glu ligand truncated at the sidechain, i.e., excluding Cα and backbone atoms (Supporting Information Figure S1). The active site model of the vanadyl mimic was mostly comparable to the native active site model except for an oxo moiety in the axial position and a succinate ligand in place of αKG (Supporting Information Figure S1). Hydrogen atoms were then added to the extracted active sites using Avogadro v1.2.0[103] (Supporting Information Figure S1). The metal-distal carboxylate oxygen atoms of αKG and succinate and the Nδ atoms of His ligands were also protonated, resulting in active site models with a neutral charge (Supporting Information Figure S1). All the heavy atoms in the final active site models were held fixed, and the added hydrogen atoms were optimized with UFF[104]. The isomers of the active sites containing water, O_2, oxo, hydroxo, and monodentate as well as bidentate succinate ligands were generated with molSimplify[105], which uses OpenBabel[106,107] as a backend. The crystal structures were used as starting points to generate additional intermediates: the vanadium or iron center was replaced by the other metal (i.e., Fe in place of V for oxo and hydroxo, V in place of Fe for water and O_2) to generate the remaining initial geometries.

All constrained geometry optimizations were performed in ORCA[108] v.4.0.1.2 and v.4.2.1 with the generalized gradient approximation (GGA) global hybrid PBE0[109] (with 25% exchange)

density functional and the def2-TZVP basis set[110]. Semi-empirical D3[111] dispersion correction with Becke–Johnson[112] damping was incorporated in these optimizations. All optimizations were carried out using the BFGS algorithm in redundant internal coordinates with default thresholds of 5×10^{-6} hartree for self-consistent field (SCF) convergence and 3×10^{-4} hartree/bohr for the maximum gradient. In all optimizations, the methyl carbon atoms of all His and Glu ligands, the five heavy atoms of succinate, and the heavy atoms in the metal-distal carboxylate group of αKG were held fixed to mimic the ligand positions in the enzyme (Supporting Information Figure S2). Closed-shell singlet calculations were carried out in a spin-restricted formalism while all open-shell calculations were simulated as unrestricted calculations (Supporting Information Table S1). Geometry optimizations of the active site isomers were carried out in both the gas phase and implicitly solvated with a dielectric value, $\varepsilon = 10$, approximately mimicking the protein environment. Conductor-like polarizable continuum model[113] (C-PCM) solvation energies using the conductor-like screening solvent model (COSMO)-type epsilon function were used to perform implicitly solvated optimizations. As observed in prior work[88], the inclusion of solvent environment effects through implicit solvent alters most gas-phase geometries very little, i.e., most bond length differences are less than 0.03 Å while a few outliers have larger changes (Supporting Information Table S2). Hence, we carry out further analyses only in the gas phase. All initial and optimized structures for gas-phase optimizations are provided in the Supporting Information.

Following the protocol from prior work[88], initial geometries to generate isomerization reaction coordinates (RCs) were constructed from the PBE0/def2-TZVP optimized geometries of active site isomers by rotating oxo/hydroxo with respect to the axial His in 1° increments of the angle formed by the oxo, the metal center (i.e., Fe, V), and the nitrogen of the axial His (Supporting Information Figure S3). Constraints were employed for each of the isomerization RCs and

constrained optimizations were performed along the chosen RC for both iron and vanadium metal centers at the PBE0/def2-TZVP level of theory in ORCA v.4.0.1.2 (Supporting Information Table S3 and Figure S4). To understand the effect of different metal centers for a given geometry, single-point calculations were obtained on optimized geometries of Fe intermediates by replacing Fe with V and vice versa. High-energy structures along the RCs were used to obtain vibrational frequencies. Numerical Hessian calculations were carried out at the same level of theory, and the Hessian was computed using the central difference approach after 6*N* atomic displacements. The presence of an imaginary frequency along the RC confirmed that the high-energy structure corresponded to a transition state. Multiwfn[114] was used to perform Mayer bond order analysis in order to quantify the strength of binding of αKG, monodentate, and bidentate succinate to both iron and vanadium metal centers.

3. Reaction Mechanism.

Prior work based on crystallographic data[84,87,115] and spectroscopic studies[116-119] along with computational studies[120,121] of non-heme Fe(II) α-KG dependent hydroxylases and the related non-heme Fe(II) dioxygenases[33,71,122] has led to the proposal of the following mechanism[1,29,42,102,123] in the catalytic cycle of non-heme hydroxylases. In its resting state, the Fe(II) hexa-coordinated active site consists of three water molecules and a 2-His-1-carboxylate (Asp/Glu) facial triad where Fe(II) is bound to two His residues and an Asp/Glu residue (Supporting Information Figure S5). The first step in the catalytic cycle is the binding of the bidentate αKG co-substrate to the iron center (**1**) which results in the displacement of two water molecules from the active site (Figure 1). When the native substrate enters the binding pocket in the proximity of Fe(II), the remaining water molecule is also displaced, resulting in a five-coordinate square pyramidal geometry around iron (Supporting Information Figure S5). This is followed by the binding of molecular oxygen (**2**) to

iron, which immediately attacks the carbonyl carbon of the bidentate αKG ligand, leading to O–O bond cleavage and oxidative decarboxylation of the bidentate αKG (Figure 1 and Supporting Information Figure S5). This catalytic step results in the formation of a highly reactive terminal Fe(IV)=O intermediate (**3**) along with the succinate co-substrate, which has a carboxylate group that can bind iron in a monodentate or bidentate fashion (Figure 1).

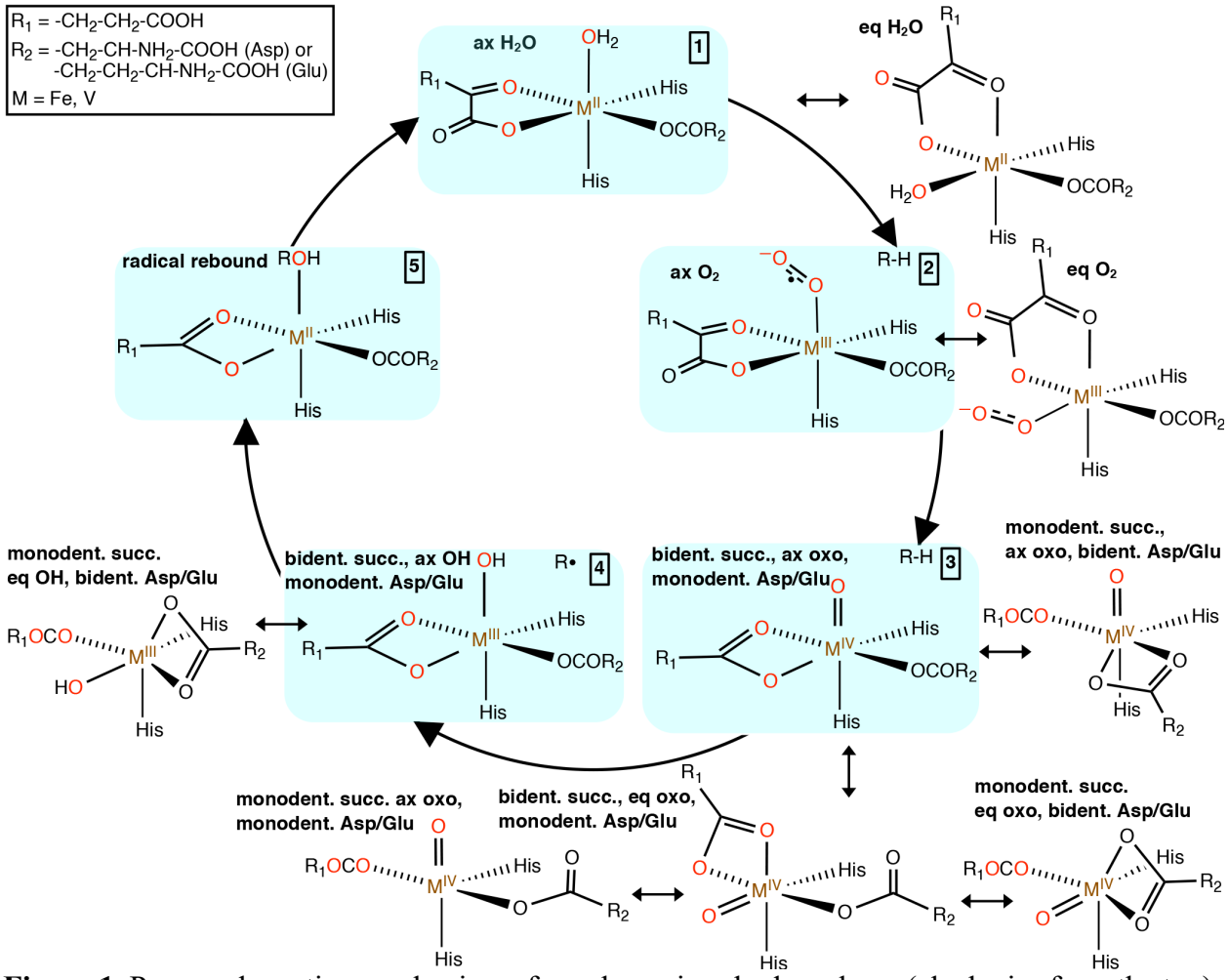

Figure 1. Proposed reaction mechanism of non-heme iron hydroxylases (clockwise from the top): the intermediates with water loosely bound to the iron center (**1**); O_2 bound to the iron center (**2**); oxo and succinate (**3**); hydroxo bound to iron (**4**); and radical rebound intermediate (**5**) are shown. Fe(II)–H_2O and Fe(III)–O_2 each have two isomers: axial (ax) and equatorial (eq) H_2O/O_2. Fe(IV)=O and Fe(III)–OH intermediates each have six isomers: (i) bidentate (bident.) succinate (succ.), axial oxo/OH, monodentate (monodent.) Asp/Glu (ii) bidentate succinate, equatorial oxo/OH, monodentate Asp/Glu (iii) monodentate succinate, axial oxo/OH, bidentate Asp/Glu (iv) monodentate succinate, equatorial oxo/OH, bidentate Asp/Glu (v) monodentate succinate, axial oxo/OH, monodentate Asp/Glu (vi) monodentate succinate, equatorial oxo/OH, monodentate

Asp/Glu. The metal, M = Fe, V, is shown in brown, and the oxidation state of metal in each intermediate is specified.

The fleeting Fe(IV)=O intermediate (**3**) then abstracts a hydrogen atom from the substrate through homolytic cleavage of a substrate C–H bond, forming a radical substrate species and an Fe(III)–OH intermediate (**4**) (Figure 1). This rate-determining hydrogen atom transfer (HAT) step is followed by recombination of the substrate radical with the hydroxyl group of the Fe(III)–OH intermediate during the radical rebound step of the catalytic cycle to form the product (**5**) (Figure 1 and Supporting Information Figure S5). After the release of the hydroxylated product and succinate and rebinding of three water molecules to iron, the active site goes back to its resting state (Supporting Information Figure S5).

Isomerization is feasible for all the intermediates formed during the catalytic cycle (Figure 1). While water and molecular oxygen in intermediates (**1**) and (**2**) are represented in axial positions due to the frequency with which this isomer is observed in crystal structures of hydroxylases[119,122-124], these intermediates can also have equatorial configurational isomers where water and molecular oxygen are in equatorial positions (Figure 1). In Fe(IV)=O and Fe(III)–OH intermediates, the active site can have a six-coordinate tetragonal or a five-coordinate square pyramidal geometry around iron depending on whether succinate and Asp/Glu are coordinated to iron in a bidentate or monodentate configuration (Figure 1 and Supporting Information Figure S6). In the case of a hexa-coordinated iron active site with bidentate succinate, Asp/Glu is monodentate, and the oxo or hydroxo moieties can be present in axial or equatorial positions, resulting in two configurational isomers (Figure 1 and Supporting Information Figure S6). Two such isomers can also be constructed when Asp/Glu is bidentate and succinate is monodentate (Figure 1 and Supporting Information Figure S6). Additionally, these two configurational isomers can be formed

when we have a penta-coordinated iron active site where both succinate and Asp/Glu are monodentate (Figure 1 and Supporting Information Figure S6). Overall, given that both succinate and Asp/Glu can bind to iron in either a monodentate or bidentate fashion, we potentially have a total of six configurational isomers for intermediates (**3**) and (**4**) (Figure 1 and Supporting Information Figure S6).

Isomerization[51,52] of the reactive Fe(IV)=O and Fe(III)–OH intermediates, in combination with substrate positioning[46,116,125], is believed to play an important role in reaction selectivity of non-heme Fe(II) enzymes. Due to the fleeting nature of these intermediates, vanadyl mimics[73,84] are commonly used in experiments to understand the structure of these intermediates. Evaluating substrate distances and angles for the preferred M(IV)=O and M(III)–OH isomers (M = Fe, V) can help us better understand the reliability of vanadyl mimics of native non-heme iron enzymes as well as the enzyme's hydroxylation activity.

4. Results and Discussion.

4.1. Spin States and Isomer Energetics for Vanadium-Based Mimics of Fe Hydroxylases.

Fe and V differ in terms of accessible spin states for all active-site intermediates, which could potentially mean that the most favorable structures are different for Fe and V intermediates (Supporting Information Table S1). To understand the effect of ground spin states on geometries and isomer energetics of the key M(IV)=O and M(III)–OH (M = Fe, V) intermediates in hydroxylases, we study active-site isomers for Fe and V intermediates in their corresponding HS (only for Fe), IS, and LS states (Supporting Information Table S1). Although Fe(IV)=O and Fe(III)–OH where Fe is d^4 and d^5, respectively, can access all three spin states, i.e., HS quintet/sextet, IS triplet/quartet, and LS singlet/doublet states, we find that both intermediates

strongly prefer an HS ground state consistent with prior experimental and computational studies[33,75,126] (Supporting Information Table S4). However, V(IV)=O where V is d^1 can only access the LS doublet state, and while V(III)–OH where V is d^2 can access IS triplet and LS singlet states, it strongly prefers an IS ground state (Supporting Information Table S4).

We study isomers of M(IV)=O and M(III)–OH intermediates for Fe and V because identifying the most stable isomers could provide valuable structural information about preferred substrate distances and angles from the metal-oxo/hydroxo moiety. We identify stable isomers in the ground spin state for all Fe and V oxo/hydroxo intermediates and find that the most stable M(IV)=O isomers differ between Fe and V (Figure 2). Although crystal structures with ferryl intermediates of non-heme iron hydroxylases are, as expected, not available, crystal structures with vanadyl intermediates show an axial oxo isomer with bidentate succinate and monodentate Glu as the most favored isomer.[85,87] In our computational studies, while Fe(IV)=O prefers an axial oxo isomer with bidentate Glu to an equatorial oxo isomer with bidentate succinate by over 3 kcal/mol, V(IV)=O shows comparable energies for both isomers along with the isomer found in crystal structures of vanadyl mimics (Figure 2). Energetic differences between the most stable bidentate and monodentate succinate/Glu Fe(IV)=O isomers is smaller, i.e., ca. 3 kcal/mol, suggesting a possibility for equilibration between bidentate and monodentate Glu (Figure 2). However, the monodentate succinate structure of V(IV)=O with an axial oxo and monodentate Glu is extremely unstable and can only be optimized with the use of additional geometric constraints, indicating that this structure may never be observed (Figure 2). We also observe that Fe(IV)=O isomers with axial oxo are energetically more favorable than their equatorial oxo counterparts, while both axial and equatorial oxo isomers are comparable in energy for V(IV)=O (Figure 2). Among Fe(IV)=O isomers with equatorial oxo, we find that bidentate succinate (i.e., with a monodentate Glu) is

strongly preferred over bidentate Glu (i.e., with a monodentate succinate) by ca. 9 kcal/mol (Figure 2). This is consistent with prior calculations[127] where, in the equatorial oxo isomer, Glu is found to bind in a monodentate fashion with one of the Fe–O_{Glu} bonds much longer than the other. On the contrary, these isomers are comparable in energy for V(IV)=O, indicating the possibility of experimentally observing an equatorial oxo isomer with bidentate Glu when vanadyl mimics are used, which incorrectly suggests the favorability of this isomer for Fe(IV)=O (Figure 2). These differences in energetic preferences of M(IV)=O isomers demonstrate that using vanadyl in place of native non-heme iron hydroxylases may not lead to valid structural mimicry.

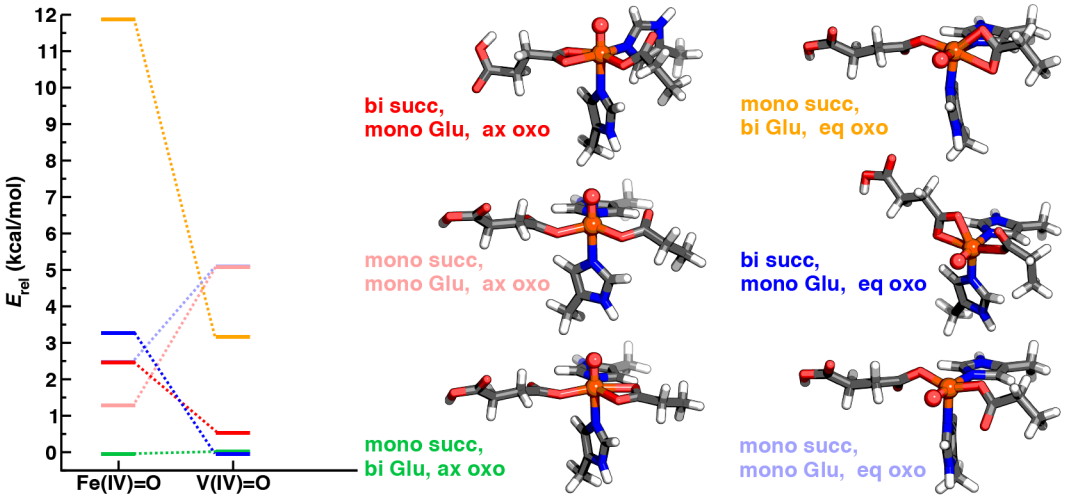

Figure 2. PBE0/def2-TZVP energies (E_{rel}) of isomers of M(IV)=O (M = Fe, V) intermediates shown relative to the most stable isomer for each intermediate in its ground spin state. Representative structures of Fe(IV)═O isomers are shown in the insets and labeled. (Top to bottom, left) Isomers are axial (ax) oxo, bidentate (bi) succinate (succ), monodentate (mono) Glu; axial oxo, monodentate succinate, monodentate Glu; axial oxo, monodentate succinate, bidentate Glu. (Top to bottom, right) Isomers are equatorial (eq) oxo, monodentate succinate, bidentate Glu; equatorial oxo, bidentate succinate, monodentate Glu; equatorial oxo, monodentate succinate, monodentate Glu. Hydrogen, carbon, nitrogen, oxygen, and iron are shown in white, gray, blue, red, and brown, respectively.

Study of M(III)–OH isomers that are formed after HAT reveals that the most stable M(III)–OH isomer is same for both Fe and V (Figure 3). Contrary to our observations for M(IV)=O

isomers, the relative energetic favorability of M(III)–OH isomers is consistent between Fe and V with smaller differences in isomer energetics (Figure 3). We also find that the metal-hydroxo moiety forms a hydrogen bond (HB) with Glu in most isomers for both Fe and V (Figure 3). Energetic comparison of a given isomer, e.g., axial OH with bidentate succinate and monodentate Glu, with and without an HB between the hydroxo moiety and Glu reveals that the HB stabilizes the Fe(III)–OH isomer by ca. 4 kcal/mol (Figure 3). However, no additional energetic stability is observed for the corresponding V(III)–OH isomers, suggesting weaker HBs in vanadium-based mimics (Figure 3). Thus, despite the comparable relative energies of minimal models of the Fe and V active sites, differences in HB interactions between Fe and V hydroxo intermediates could imply differences in isomerization of M(III)–OH isomers, which further determine the rebound reaction step in the catalytic cycle.

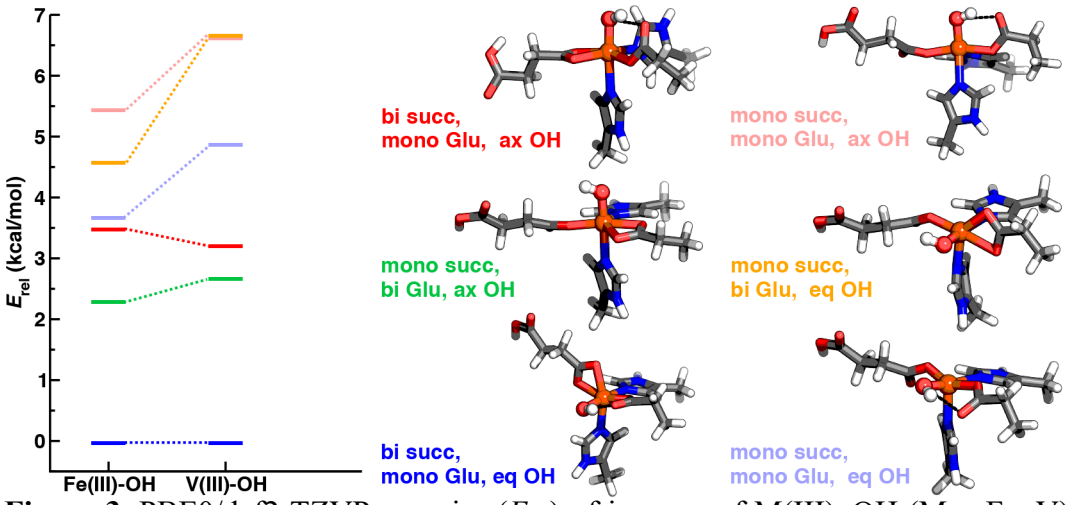

Figure 3. PBE0/def2-TZVP energies (E_{rel}) of isomers of M(III)–OH (M = Fe, V) intermediates shown relative to the most stable isomer for each intermediate in its ground spin state. Representative structures of Fe(III)–OH isomers are shown in the insets and labeled. (Top to bottom, left) Isomers are axial (ax) OH, bidentate (bi) succinate (succ), monodentate (mono) Glu; axial OH, monodentate succinate, bidentate Glu; equatorial (eq) OH, bidentate succinate, monodentate Glu. (Top to bottom, right) Isomers are axial OH, monodentate succinate, monodentate Glu; equatorial OH, monodentate succinate, bidentate Glu; equatorial OH, monodentate succinate, monodentate Glu. Hydrogen, carbon, nitrogen, oxygen, and iron are shown in white, gray, blue, red, and brown, respectively.

Next, we analyze differences in metal–ligand (M–L) bond lengths to identify if they are sensitive reporters of the differences in bonding between the favored spin states for Fe and V isomers of M(IV)=O and M(III)–OH. M-oxo bonds in HS and IS Fe(IV)=O isomers are longer than those in LS V(IV)=O isomers by ca. 0.04 Å and 0.03 Å, respectively, but LS Fe-oxo bonds are more comparable to V-oxo bonds, i.e., they differ by < 0.01 Å, highlighting that differences in spin state are likely the main source of differences in isomer structure and potentially energetics (Supporting Information Table S5). All other M–L bonds of Fe and V intermediates, regardless of spin state, differ by < 0.10 Å except for specific isomers with elongated V–N_{His}, V–O_{suc}, or V–O_{Glu} bonds (Supporting Information Tables S5–S6). Consistent with observations on halogenases[88], relative isomer energetics differ significantly between HS Fe(IV)=O and LS V(IV)=O intermediates, while they are comparable between IS Fe(IV)=O and LS V(IV)=O intermediates (Figure 2 and Supporting Information Table S7 and Figure S7). Further study of isomer geometries reveals that the orientation of the Glu carboxylate can change isomer energetics by 1–4 kcal/mol depending on the denticity of succinate for both Fe and V intermediates (Supporting Information Figure S8). Isomers where the free Glu carboxylate oxygen is pointed away from succinate are more energetically favorable than those with the free Glu carboxylate oxygen oriented towards succinate (Supporting Information Figure S8). This energetic preference becomes significant in the presence of bidentate succinate likely due to a combination of steric and electrostatic effects.

We then compare Fe and V intermediates of non-heme hydroxylases to those of halogenases to understand if V-mimics are more faithful in one of the two enzyme classes. We observe considerable differences between Fe and V intermediates for both hydroxylases and halogenases, but the nature of these differences is distinct in the two enzyme classes. The range of

isomer energetics spanned by the native ferryl species in halogenases[88] is much smaller relative to hydroxylases, i.e., 4 kcal/mol vs 12 kcal/mol, while the opposite trend is observed for isomer energetics of their vanadyl mimics, i.e., 18 kcal/mol vs 5 kcal/mol (Figure 2). This shows that while all halogenase Fe(IV)=O isomers are generally accessible and interconvertible, some of the vanadyl isomers incorrectly imply highly unfavorable energetics for the most favored native iron isomers[88]. On the contrary, vanadyl mimics of hydroxylases incorrectly suggest favorable energetics for one of the most energetically unfavorable ferryl isomers (Figure 2). The nature of differences between Fe intermediates and their V mimics for hydroxylases vs halogenases are likely the result of size difference between the coordinating carboxylate residue in hydroxylases and the active site halide in halogenases. Furthermore, the carboxylate residue in hydroxylases can bind in a monodentate or bidentate fashion which could lead to additional steric or electrostatic interactions (i.e., with respect to other active-site ligands), which are not observed in halogenases with a monodentate halide ligand, as we will explore in more detail next. For both halogenases and hydroxylases, however, vanadyl mimics of monodentate succinate isomers exhibit strongly unfavorable energies, meaning that they may not be observed experimentally, although these isomers for the native Fe(IV)=O intermediate are energetically favorable. These observations show that the energetics of the native ferryl intermediates are not accurately captured by their vanadyl mimics, suggesting that vanadyl structures are not faithful mimics of ferryl intermediates in C–H activation.

4.2. Differences in Fe and V Isomerization Barriers between Metal-Oxo/Hydroxo Isomers.

We study the isomerization reaction coordinate (RC) in the M(IV)=O intermediate for both Fe and V, and compare their energy landscapes. When choosing a starting point for this isomerization, we note that while the bidentate Glu isomer is slightly more stable than the

monodentate Glu isomer, we study active site isomerization for isomers where succinate or Glu or both are monodentate. This modification allows for more flexibility in the active site to enable isomerization of the reacting moiety, i.e., oxo/hydroxo. Importantly, we found small energetic differences between monodentate and bidentate succinate/Glu isomers for the Fe(IV)=O intermediate, i.e., ca. 3 kcal/mol (Figure 2).

We study two closely related isomerization RCs for monodentate succinate/Glu isomers of both Fe(IV)=O and V(IV)=O intermediates to compare the energetic differences for the two metals. The first RC connects the axial and equatorial oxo isomers as a function of N_{His}–M=O angle where both succinate and Glu remain monodentate during isomerization, and we note significant differences between Fe and V (Figure 4 and Supporting Information Figure S4). For Fe, isomerization from axial oxo to equatorial oxo is separated by a transition state (TS) with a high energy barrier of 10.4 kcal/mol for Fe(IV)=O (Figure 4). The global minimum on the RC (N_{His}–Fe=O angle: 176°) corresponds to the axial oxo isomer and the local minimum (N_{His}–Fe=O angle: 90°) corresponds to the equatorial oxo isomer (Figure 4). We characterize this TS by observing a single imaginary frequency along the angular RC mode (N_{His}–Fe=O angle: 124°). However, for V(IV)=O, this isomerization is barrierless, and the minimum energy structure positions the oxo moiety between the axial position and equatorial plane, i.e., N_{His}–V=O angles: 147° (Figure 4). The energetics of axial and equatorial oxo isomers observed along the isomerization RCs for Fe and V differ by ca. 4 kcal/mol, which is slightly higher than that observed during free optimizations (Figure 3 and Figure 4). The small increase in energetic differences along the RCs could be the result of additional constraints used during the construction of RCs and the differences in Glu orientation, i.e., the carboxylate group of Glu pointing towards succinate along the RCs vs pointing away from succinate during free optimizations (Figure 3 and Figure 4). We

also obtain largely similar isomerization RCs for Fe and V where Glu is forced to remain monodentate while succinate is allowed to be monodentate or bidentate, and we find that succinate prefers to remain monodentate along these RCs even in the absence of constraints on succinate (Figure 4 and Supporting Information Figure S9).

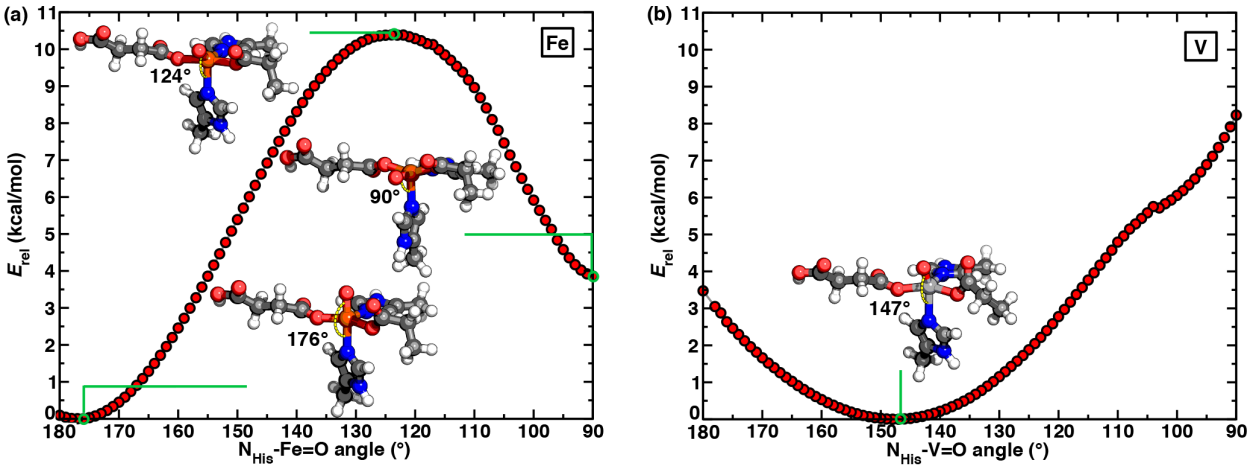

Figure 4. Reaction coordinates for isomerization between axial oxo and equatorial oxo with monodentate succinate and monodentate Glu for (a) Fe and (b) V active sites. The geometries corresponding to minima and transition states are shown as insets. The N_{His}–M=O angles (in °, M=Fe, V) are indicated as yellow dashed curves in the inset structures. Hydrogen, carbon, nitrogen, oxygen, vanadium, and iron are shown in white, gray, blue, red, silver, and brown, respectively.

The second RC also connects the monodentate succinate isomers of axial oxo and equatorial oxo as a function of the N_{His}–M=O angle but, unlike the previous RC, allows Glu to bind the metal either in a monodentate or bidentate fashion (Supporting Information Figures S10–S11). For both Fe and V, Glu prefers to be bidentate when oxo is closer to the axial position or the equatorial plane but becomes monodentate when oxo is midway between the axial position and the equatorial plane (Supporting Information Figure S11). The change in denticity of Glu is captured by the discontinuities in the isomerization energy landscape, i.e., at N_{His}–M=O angle of 143° for Fe and 149° for Fe V, where the sudden change to a more favorable energy corresponds

to the change in Glu binding from monodentate to bidentate (Supporting Information Figure S10). These modified isomerization RCs of Fe and V with flexible Glu binding are qualitatively similar to those obtained with both monodentate succinate and monodentate Glu except that the isomerization barrier for Fe(IV)=O is higher by 3.0 kcal/mol when Glu is not constrained to be monodentate (Figure 4 and Supporting Information Figure S10). This suggests that although the isomerization barrier could be higher in the enzyme active site if bidentate Glu coordination is enforced throughout the catalytic cycle by interactions with the protein environment, it can be lowered by forcing Glu to remain monodentate for the entirety of the reaction through alternative favorable interactions. For example, hydrogen bonding (HB) interactions between the carboxylate of Glu and nearby residues could force Glu to remain monodentate and enable isomerization with a lower barrier. For a representative hydroxylase, VioC,[10,85,101,102] Glu bound to the metal center can potentially form HBs with the substrate, L-arginine, or a nearby Arg334 residue that would force Glu to remain monodentate. Similarly, in TauD[119], Asp bound to the metal center can potentially HB with the nearby Arg270 residue, thus remaining monodentate.

We also obtain isomerization RCs in which we swap one metal center into the geometry of the alternate metal, i.e., Fe(IV)=O as single-point calculations of the optimized geometries along the isomerization RC of V(IV)=O and vice versa (Supporting Information Figure S12). These frozen RCs are similar to the relaxed RCs for both Fe and V, except for the small increase in energetics owing to the fully constrained geometries, suggesting that geometric structure plays only a relatively minor role relative to electronic structure and spin state differences of Fe and V play in isomer energetics (Supporting Information Figure S12). Overall, the isomerization RCs connecting axial oxo and equatorial oxo isomers differ significantly between Fe and V, indicating

that vanadyl mimics of native non-heme iron hydroxylases fail to capture isomerization barriers and energy landscapes accurately.

Next, we also obtain isomerization RCs for M(III)–OH intermediates which connect axial and equatorial hydroxo isomers as a function of N_{His}–M–OH angle where both succinate and Glu remain monodentate during isomerization (Supporting Information Figure S13). We obtain two RCs for each metal: RC_{OH1} where hydroxo is hydrogen bonded to Glu throughout the RC and RC_{OH2} where hydroxo does not hydrogen bond with Glu (Supporting Information Figure S13). Examination of these RCs reveals considerable differences in RCs obtained for Fe and V. While for Fe, the isomer with equatorial OH is found to be the global minimum and the isomer with OH placed mid-way between equatorial and axial positions is found to be a local minimum along RC_{OH1}, the stability of the minima is reversed for V (Supporting Information Figure S13). For Fe and V, both minima are comparable in energy along $RC_{OH1,}$ consistent with the isomer energetics observed during free optimizations (Figure 3 and Supporting Information Figure S13). Isomerization from the local to global minimum is accompanied by a minor barrier of 1.5 kcal/mol for Fe and a larger barrier of 3 kcal/mol for V (Supporting Information Figure S13). Comparison of RC_{OH1} and RC_{OH2} reveals significant differences between these RCs both in terms of energetics and preferred minimum energy geometries (Supporting Information Figure S13). For instance, along RC_{OH2}, the Fe(III)–OH isomer with OH placed mid-way between axial and equatorial positions is the global minimum and the isomer with OH closer to an axial position is a local minimum (Supporting Information Figure S13). The transition from global to local minimum along RC_{OH2} is also accompanied by a minor barrier of ca. 1 kcal/mol for Fe (Supporting Information Figure S13). The isomerization along RC_{OH2} for V(III)–OH isomer shows one global minimum and two local minima, all of which are comparable in energy with a difference of less

than 1 kcal/mol (Supporting Information Figure S13). The energetic barriers to move from one minimum to another are also relatively minor, i.e., ca. 1 kcal/mol (Supporting Information Figure S13). Overall, given the more favorable energetics of RC_{OH1} relative to RC_{OH2}, we can expect that hydroxo isomerization would be accompanied by hydrogen bonding interactions between hydroxo and Glu, although the presence of the hydrogen bond does modestly increase isomerization barriers (Supporting Information Figure S13).

In comparison to previously studied halogenases,[88] barriers for isomerization between axial and equatorial Fe-oxo isomers is higher for hydroxylases by ca. 5 kcal/mol, suggesting that isomerization from axial oxo to equatorial oxo is more difficult in hydroxylases relative to halogenases. As the size of the carboxylate ligand played a role in distinguishing the relative isomer energetics of halogenases and hydroxylases (see Sec. 4.1), it may similarly affect differences in isomerization barriers. Isomerization of the oxo moiety forces Glu to change its orientation along the RC. We will examine the possibility that this might result in Glu having unfavorable orientations during oxo isomerization, leading to higher isomerization barriers in Sec. 4.4. Comparison of hydroxo isomerization RCs also reveals considerable differences between hydroxylases and halogenases. In contrast to halogenases,[88] OH isomerization in hydroxylases can take place through two pathways: one with HBs between OH and Glu, and the other without hydrogen bonding interactions. While the latter RC is qualitatively similar to the OH isomerization energy landscape observed in halogenases, it is likely that the former RC (i.e., with HBs between OH and Glu) would be preferred due to its overall favorable energetics. For both hydroxylases and halogenases overall, angular RCs and energy landscapes differ significantly between Fe and their V mimics, demonstrating that conclusions on the ease of active site isomerization will be metal-

dependent and reinforcing the limits of using vanadyl species to understand catalysis in these enzyme classes.

4.3. Binding Strength of Succinate and Glu in Comparison to αKG.

The formation of monodentate succinate and/or monodentate Glu is likely necessary for isomerization of M(IV)=O intermediates. However, the most energetically favorable ferryl isomers prefer a bidentate Glu or bidentate succinate (Figure 2). In order to quantify the differences in the binding strength of monodentate and bidentate succinate/Glu to the metal centers, i.e., Fe and V, we perform Mayer bond order analysis, a quantum mechanical assessment of bond order. Additionally, we compare the binding strengths of succinate and Glu to that of αKG, which consistently binds in a bidentate fashion.

Comparison of binding strengths of bidentate and monodentate succinate/Glu to Fe and V confirms that bidentate succinate and Glu bind more strongly than their monodentate counterparts for both metals, i.e., we observe Mayer bond orders of 0.82 vs 0.63 for binding to Fe, and a larger difference in bond orders of 0.94 vs 0.56 for binding to V (Figure 5). However, their binding strength is much weaker than that of the bidentate αKG for both metals, which could in part be a result of the differences in structures (Figure 5). For example, the M–O distances of Fe/V to both O atoms of αKG are shorter by ca. 0.20 Å in comparison to average M–O distances for bidentate succinate (Figure 5). We observe comparable binding strengths of both carboxylate ligands, i.e., monodentate (bidentate) Glu binds as strongly as monodentate (bidentate) succinate for Fe and V (Figure 5). Comparison of ligand binding strengths between oxo and hydroxo intermediates reveals that, relative to oxo isomers, the binding strength of monodentate Glu is reduced in hydroxo

isomers for both metals owing to hydrogen bonding interactions between the hydroxo moiety and Glu (Figure 5 and Supporting Information Figure S14).

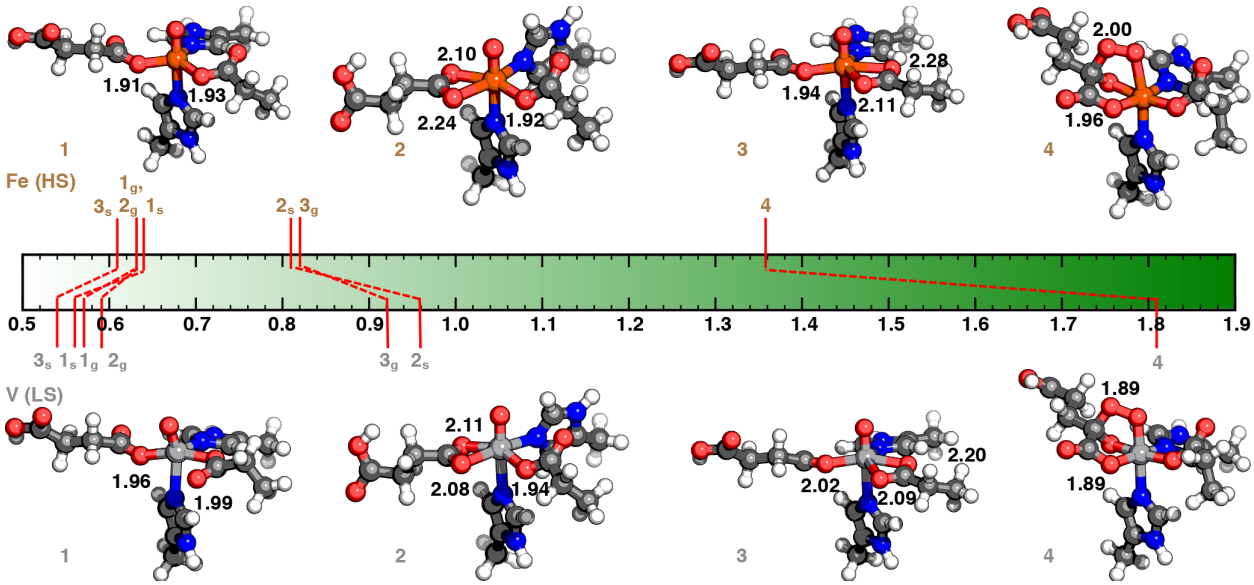

Figure 5. Scale demonstrating the Mayer bond orders of metal–Glu (g), metal–succinate (s), and metal–αKG bonds of ground state high-spin (HS) Fe (top) and low-spin (LS) V (bottom) intermediates with monodentate Glu/succinate and bidentate Glu/succinate/ αKG. The four intermediates shown are (1) M(IV)=O with monodentate succinate and monodentate Glu, (2) M(IV)=O with bidentate succinate and monodentate Glu, (3) M(IV)=O with monodentate succinate and bidentate Glu, and (4) M(III)–O_2 with bidentate αKG. The corresponding M–O (of Glu/succinate/αKG) bond lengths (in Å) are indicated in the insets. Hydrogen, carbon, nitrogen, oxygen, vanadium, and iron are shown in white, gray, blue, red, silver, and brown, respectively.

Across all the isomers of oxo, hydroxo, and O_2-bound intermediates, we find stronger binding of bidentate succinate, bidentate Glu, and bidentate αKG in V intermediates relative to Fe intermediates (Figure 5). This difference in binding strength is most significant for the binding of αKG to the metal center. αKG binds more strongly to V than to Fe (Mayer bond order: 1.81 vs 1.36), likely due to the LS ground state for V in comparison to the HS ground state for Fe (Figure 5). However, in oxo and hydroxo isomers, the binding strengths of monodentate succinate and monodentate Glu are comparable between Fe and V intermediates (Figure 5). From the analysis

of ligand binding strengths, we thus conclude that bidentate succinate is only slightly more strongly bound to the metal than monodentate succinate, and this trend is preserved in both Fe and V active sites. This supports the potential isomerization between isomers of M(IV)=O intermediates to enable HAT during the catalytic cycle and it suggests that V mimics should be suitable to capture this factor in isomerization.

To isolate the effect of bidentate coordination on M(IV)=O isomerization, we create artificial isomerization RCs where either succinate or Glu is constrained to its bidentate orientation along the RCs. We find that succinate/Glu cannot remain bidentate throughout the RC and must rearrange to structures with monodentate succinate/Glu, especially for N_{His}–M=O angles between 130° and 140°, to facilitate isomerization for both Fe and V (Figure 6). We also observe that for the Fe(IV)=O intermediate, when bidentate structures are feasible, RCs with bidentate Glu show more favorable energies overall relative to RCs with bidentate succinate (Figure 6). This suggests that oxo isomerization would most likely take place with bidentate Glu and monodentate succinate (Figure 6). While monodentate Glu isomers are higher in energy than bidentate Glu isomers by only 3 kcal/mol for Fe, in the isomerization RCs, we observe a larger difference of 10 kcal/mol (Figures 3 and 6). This is due to the additional constraints imposed on succinate and Glu during the isomerization RCs which result in unfavorable angles of binding between succinate/Glu and Fe, leading to increased isomer energetics (Figures 3 and 6 and Supporting Information Figure S15). For both metals, the bidentate RCs for oxo isomerization show bidentate Glu to be favorable when oxo is closer to the axial position (Figure 6). However, when oxo is closer to the equatorial plane, bidentate succinate and bidentate Glu RCs show comparable energies for Fe whereas bidentate succinate is more favorable than bidentate Glu for V (Figure 6). This suggests that the Fe-oxo species maintains a bidentate Glu in either isomer orientation, while the V-oxo species

likely has either bidentate Glu or succinate coordination depending on the isomer orientation (Figure 6). The significant differences between Fe and V RCs with bidentate succinate/Glu demonstrate that V does not accurately capture the oxo isomerization of the ferryl intermediate.

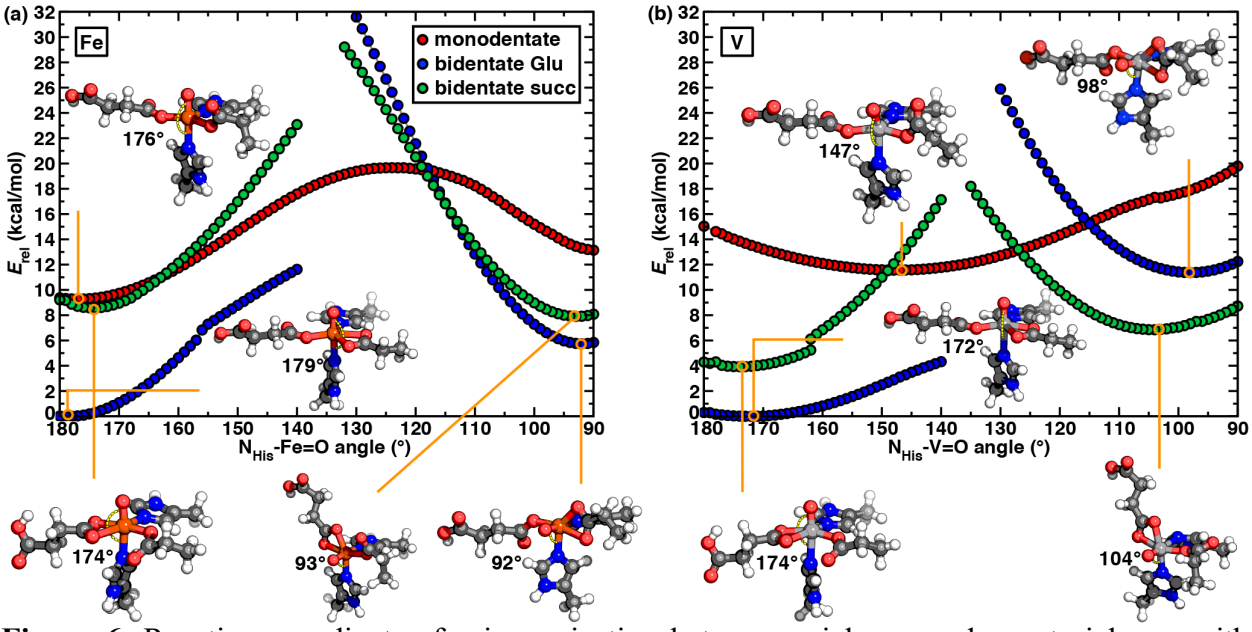

Figure 6. Reaction coordinates for isomerization between axial oxo and equatorial oxo with monodentate Glu and monodentate succinate (shown in red), bidentate Glu and monodentate succinate (shown in blue), and monodentate Glu and bidentate succinate (shown in green) for (a) Fe and (b) V active sites. The geometries corresponding to minima are shown as insets. The N_{His}–M=O angle (in °, M=Fe, V) is indicated as yellow dashed curves in the insets. Hydrogen, carbon, nitrogen, oxygen, vanadium, and iron are shown in white, gray, blue, red, silver, and brown, respectively.

In a prior study,[88] the bidentate succinate RCs for halogenases revealed that isomerization between axial and equatorial oxo could take place with bidentate succinate for the most part except for structures with N_{His}–M=O angles between 130° and 140° where succinate must bind in a monodentate fashion. Although this is largely consistent with what we observe for bidentate succinate/Glu RCs of hydroxylases, monodentate isomers are found to be energetically more favorable for structures with a larger range of N_{His}–M=O angles (Figure 6). For example, structures with N_{His}–M=O angles: 120°–160° (120°–140°) are energetically more favorable with monodentate succinate/Glu rather than bidentate succinate (Glu) (Figure 6). This is indeed

consistent with isomer energetics of Fe(IV)=O in hydroxylase models where bidentate Glu that binds through axial and equatorial sites is energetically less favorable than monodentate Glu (Figure 3). Overall, while halogenases tend to prefer oxo isomerization with bidentate succinate, hydroxylases prefer oxo isomerization with primarily bidentate Glu that binds through equatorial sites and with monodentate Glu for a considerable portion of the RC.

5. Conclusions.

While vanadyl mimics are frequently employed experimentally in place of the fleeting ferryl intermediate in C–H activation, we showed through an extensive computational study using DFT that there are crucial differences between ferryl and vanadyl intermediates in hydroxylase active site models that could be rationalized in terms of differences in their ground spin states. Our study of M(IV)=O isomers revealed not only that the most favorable metal-oxo isomers differ between Fe and V, but also that conversion between monodentate and bidentate isomers is energetically favorable for Fe but strongly unfavorable in vanadyl mimics.

To further understand the differences between Fe intermediates and their V-based mimics, we studied active site isomerization of Fe(IV)=O with monodentate succinate and monodentate Glu between axial and equatorial oxo isomers. We observed that the local and global minima for Fe(IV)=O isomers are separated by a transition state with a large barrier of ca. 10 kcal/mol that increases by 3 kcal/mol when Glu is allowed to become bidentate. This suggests that favorable interactions in the protein environment, e.g., hydrogen bonding interactions with Glu, could help reduce the isomerization barrier by forcing Glu to remain monodentate. Comparison of these isomerization barriers to those observed for halogenases[88] showed that isomerization is more difficult in hydroxylases likely due to the presence of a larger Glu/Asp residue that could be forced

into unfavorable orientations along the isomerization RC. Study of the corresponding isomerization RC for V(IV)=O reveals a significantly different barrierless energy landscape with only one minimum energy structure where oxo is located midway between the axial position and the equatorial plane. The Fe(IV)=O isomerization RC with bidentate Glu has more energetically favorable structures relative to RCs with bidentate succinate or those with monodentate structures, an effect not captured by the vanadyl mimics. Although more modest, differences were also observed in Fe(III)-OH versus V(III)-OH isomerization. Finally, we analyzed the relative bond strengths of monodentate and bidentate Glu/succinate for Fe and V in relation to the binding strength of the bidentate αKG and found that Glu and succinate bidentate binding is much weaker than αKG for both Fe and V. While differences between Fe and V were smaller, we generally found that the LS V intermediates especially for O_2-bound intermediates more strongly than the Fe counterparts.

Overall, the relative energetics of oxo isomers and isomerization RCs connecting these isomers differ even more significantly between Fe and V hydroxylases than they do for previously studied halogenases. This indicates that vanadyl mimics of native non-heme iron hydroxylases will fail to capture isomerization barriers and energy landscapes accurately. The study of various isomerization RCs sets the stage for targeted approaches to lower active-site isomerization barriers in non-heme iron hydroxylases.

ASSOCIATED CONTENT

Supporting Information. Extracted active sites of VioC and its vanadyl mimic; structures highlighting atom constraints used in geometry optimizations between implicit solvent and gas-phase optimized geometries; structures highlighting angle constraints in oxo/OH isomerization RCs; list of constraints employed in isomerization RCs; structures highlighting constraints in various isomerization RCs; structures of intermediates formed during the catalytic cycle; isomers of all four intermediates formed during the catalytic cycle; list of all possible spin states of active site intermediates; isomer spin splitting energies of oxo and OH intermediates of Fe and V; bond length differences of HS/IS/LS Fe(IV)=O and LS V(IV)=O; bond length differences of HS/IS/LS Fe(III)–OH and IS V(III)–OH; relative isomer energetics of M(IV)=O and M(III)–OH (M = Fe, V); relative isomer energetics of IS Fe(IV)=O and LS V(IV)=O; representative M(IV)=O isomers depicting unfavorable Glu orientations; isomerization with monodentate Glu and monodentate/bidentate succinate; isomerization with monodentate succinate and monodentate/bidentate Glu; representative Fe(IV)=O geometries along isomerization RC; isomerization RCs obtained as single point calculations; isomerization RCs for M(III)–OH intermediates; Mayer bond orders of hydroxo intermediates; structures of M(IV)=O isomers from optimizations vs isomerization RCs (PDF)

Initial geometries for geometry optimizations of isomers of metal-oxo and metal-hydroxo intermediates for Fe and V; optimized geometries of isomers of metal-oxo and metal-hydroxo intermediates for Fe and V; optimized geometries along the isomerization RCs of Fe(IV)=O and V(IV)=O intermediates (ZIP)

AUTHOR INFORMATION

Corresponding Author

*email:hjkulik@mit.edu

Notes

The authors declare no competing financial interest.

ACKNOWLEDGMENT

This work was supported by the National Science Foundation under grant numbers CBET-1704266 and CBET-1846426. The authors acknowledge the MIT SuperCloud and Lincoln Laboratory Supercomputing Center for providing HPC resources that have contributed to the

research results reported within this paper. This work also made use of Department of Defense HPCMP computing resources. This work was also carried out in part using computational resources from the Extreme Science and Engineering Discovery Environment (XSEDE), which is supported by National Science Foundation grant number ACI-1548562. H.J.K. holds a Career Award at the Scientific Interface from the Burroughs Wellcome Fund, an AAAS Marion Milligan Mason Award, and an Alfred P. Sloan Fellowship in Chemistry, which supported this work. The authors acknowledge Adam H. Steeves for providing critical readings of the manuscript.

References

(1) Martinez, S.; Hausinger, R. P. Catalytic Mechanisms of Fe(Ii)-and 2-Oxoglutarate-Dependent Oxygenases. *J. Biol. Chem.* **2015,** *290*, 20702-20711.
(2) Herr, C. Q.; Hausinger, R. P. Amazing Diversity in Biochemical Roles of Fe(Ii)/2-Oxoglutarate Oxygenases. *Trends Biochem. Sci.* **2018,** *43*, 517-532.
(3) Islam, M. S.; Leissing, T. M.; Chowdhury, R.; Hopkinson, R. J.; Schofield, C. J. 2-Oxoglutarate-Dependent Oxygenases. *Annu. Rev. Biochem.* **2018,** *87*, 585-620.
(4) Prakash, G. K. S.; Mathew, T.; Hoole, D.; Esteves, P. M.; Wang, Q.; Rasul, G.; Olah, G. A. N-Halosuccinimide/Bf3-H2o, Efficient Electrophilic Halogenating Systems for Aromatics. *J. Am. Chem. Soc.* **2004,** *126*, 15770-15776.
(5) Alonso, F.; Beletskaya, I. P.; Yus, M. Metal-Mediated Reductive Hydrodehalogenation of Organic Halides. *Chem. Rev.* **2002,** *102*, 4009-4091.
(6) Altus, K. M.; Love, J. A. The Continuum of Carbon-Hydrogen (C-H) Activation Mechanisms and Terminology. *Commun Chem* **2021,** *4*, 173.
(7) Berger, M. B.; Walker, A. R.; Vazquez-Montelongo, E. A.; Cisneros, G. A. Computational Investigations of Selected Enzymes from Two Iron and A-Ketoglutarate-Dependent Families. *Phys. Chem. Chem. Phys.* **2021,** *23*, 22227-22240.
(8) Loenarz, C.; Schofield, C. J. Expanding Chemical Biology of 2-Oxoglutarate Oxygenases. *Nat. Chem. Biol.* **2008,** *4*, 152-156.
(9) Price, J. C.; Barr, E. W.; Glass, T. E.; Krebs, C.; Bollinger, J. M. Evidence for Hydrogen Abstraction from C1 of Taurine by the High-Spin Fe(Iv) Intermediate Detected During Oxygen Activation by Taurine :Alpha-Ketoglutarate Dioxygenase (Taud). *J. Am. Chem. Soc.* **2003,** *125*, 13008-13009.
(10) Helmetag, V.; Samel, S. A.; Thomas, M. G.; Marahiel, M. A.; Essen, L.-O. Structural Basis for the Erythro-Stereospecificity of the L-Arginine Oxygenase Vioc in Viomycin Biosynthesis. *FEBS J.* **2009,** *276*, 3669-3682.
(11) de Visser, S. P. Trends in Substrate Hydroxylation Reactions by Heme and Nonheme Iron(Iv)-Oxo Oxidants Give Correlations between Intrinsic Properties of the Oxidant with Barrier Height. *J. Am. Chem. Soc.* **2010,** *132*, 1087-1097.
(12) de Visser, S. P. Mechanistic Insight on the Activity and Substrate Selectivity of Nonheme Iron Dioxygenases. *Chem. Rec.* **2018,** *18*, 1501-1516.

(13) Mitchell, A. J.; Zhu, Q.; Maggiolo, A. O.; Ananth, N. R.; Hillwig, M. L.; Liu, X.; Boal, A. K. Structural Basis for Halogenation by Iron- and 2-Oxo-Glutarate-Dependent Enzyme Welo5. *Nat. Chem. Biol.* **2016,** *12*, 636-640.
(14) Blasiak, L. C.; Vaillancourt, F. H.; Walsh, C. T.; Drennan, C. L. Crystal Structure of the Non-Haem Iron Halogenase Syrb2 in Syringomycin Biosynthesis. *Nature* **2006,** *440*, 368-371.
(15) Li, R.-N.; Chen, S.-L. Mechanism for the Halogenation and Azidation of Lysine Catalyzed by Non-Heme Iron Besd Enzyme. *Chem. - Asian J.* **2022,** *17*, e202200438.
(16) Agarwal, V.; Miles, Z. D.; Winter, J. M.; Eustaquio, A. S.; El Gamal, A. A.; Moore, B. S. Enzymatic Halogenation and Dehalogenation Reactions: Pervasive and Mechanistically Diverse. *Chem. Rev.* **2017,** *117*, 5619-5674.
(17) Zhang, X.; Wang, Z.; Gao, J.; Liu, W. Chlorination Hydroxylation Selectivity Mediated by the Non-Heme Iron Halogenase Welo5. *Phys. Chem. Chem. Phys.* **2020,** *22*, 8699-8712.
(18) Nam, W. High-Valent Iron(Iv)-Oxo Complexes of Heme and Non-Heme Ligands in Oxygenation Reactions. *Acc. Chem. Res.* **2007,** *40*, 522-531.
(19) Suh, Y.; Seo, M. S.; Kim, K. M.; Kim, Y. S.; Jang, H. G.; Tosha, T.; Kitagawa, T.; Kim, J.; Nam, W. Nonheme Iron(Ii) Complexes of Macrocyclic Ligands in the Generation of Oxoiron(Iv) Complexes and the Catalytic Epoxidation of Olefins. *J. Inorg. Biochem.* **2006,** *100*, 627-633.
(20) Chen, K.; Costas, M.; Kim, J.; Tipton, A. K.; Que, L. Olefin Cis-Dihydroxylation Versus Epoxidation by Non-Heme Iron Catalysts: Two Faces of an Feiii-Ooh Coin. *J. Am. Chem. Soc.* **2002,** *124*, 3026-3035.
(21) Mukherjee, M.; Dey, A. Electron Transfer Control of Reductase Versus Monooxygenase: Catalytic C-H Bond Hydroxylation and Alkene Epoxidation by Molecular Oxygen. *ACS Cent. Sci.* **2019,** *5*, 671-682.
(22) Usharani, D.; Janardanan, D.; Shaik, S. Does the Taud Enzyme Always Hydroxylate Alkanes, While an Analogous Synthetic Non-Heme Reagent Always Desaturates Them? *J. Am. Chem. Soc.* **2011,** *133*, 176-179.
(23) Dong, G.; Lu, J.; Lai, W. Insights into the Mechanism of Aromatic Ring Cleavage of Noncatecholic Compound 2-Aminophenol by Aminophenol Dioxygenase: A Quantum Mechanics/Molecular Mechanics Study. *ACS Catal.* **2016,** *6*, 3796-3803.
(24) Solomon, E. I.; Decker, A.; Lehnert, N. Non-Heme Iron Enzymes: Contrasts to Heme Catalysis. *Proc. Natl. Acad. Sci. U. S. A.* **2003,** *100*, 3589-3594.
(25) Kivirikko, K. I.; Myllyharju, J. Prolyl 4-Hydroxylases and Their Protein Disulfide Isomerase Subunit. *Matrix Biology* **1998,** *16*, 357-368.
(26) Ivan, M.; Kondo, K.; Yang, H.; Kim, W.; Valiando, J.; Ohh, M.; Salic, A.; Asara, J. M.; Lane, W. S.; Kaelin, W. G., Jr. Hifα Targeted for Vhl-Mediated Destruction by Proline Hydroxylation: Implications for O2 Sensing. *Science* **2001,** *292*, 464-468.
(27) Jaakkola, P.; Mole, D. R.; Tian, Y.-M.; Wilson, M. I.; Gielbert, J.; Gaskell, S. J.; von Kriegsheim, A.; Hebestreit, H. F.; Mukherji, M.; Schofield, C. J.; Maxwell, P. H.; Pugh, C. W.; Ratcliffe, P. J. Targeting of Hif-A to the Von Hippel-Lindau Ubiquitylation Complex by O2-Regulated Prolyl Hydroxylation. *Science* **2001,** *292*, 468-472.
(28) Gerken, T.; Girard, C. A.; Tung, Y.-C. L.; Webby, C. J.; Saudek, V.; Hewitson, K. S.; Yeo, G. S. H.; McDonough, M. A.; Cunliffe, S.; McNeill, L. A.; Galvanovskis, J.; Rorsman, P.; Robins, P.; Prieur, X.; Coll, A. P.; Ma, M.; Jovanovic, Z.; Farooqi, I. S.; Sedgwick, B.; Barroso, I.; Lindahl, T.; Ponting, C. P.; Ashcroft, F. M.; O'Rahilly, S.; Schofield, C. J. The

Obesity-Associated Fto Gene Encodes a 2-Oxoglutarate-Dependent Nucleic Acid Demethylase. *Science* **2007,** *318*, 1469-1472.
(29) Hausinger, R. P. Fe(Ii)/Alpha-Ketoglutarate-Dependent Hydroxylases and Related Enzymes. *Crit Rev Biochem Mol* **2004,** *39*, 21-68.
(30) Walsh, C. T. The Chemical Versatility of Natural-Product Assembly Lines. *Acc. Chem. Res.* **2008,** *41*, 4-10.
(31) Blunt, J. W.; Copp, B. R.; Hu, W.-P.; Munro, M. H. G.; Northcote, P. T.; Prinsep, M. R. Marine Natural Products. *Nat. Prod. Rep.* **2009,** *26*, 170-244.
(32) Gao, S.-S.; Naowarojna, N.; Cheng, R.; Liu, X.; Liu, P. Recent Examples of a-Ketoglutarate-Dependent Mononuclear Non-Haem Iron Enzymes in Natural Product Biosyntheses. *Nat. Prod. Rep.* **2018,** *35*, 792-837.
(33) Krebs, C.; Galonic Fujimori, D.; Walsh, C. T.; Bollinger Jr., J. M. Non-Heme Fe(Iv)–Oxo Intermediates. *Acc. Chem. Res.* **2007,** *40*, 484-492.
(34) Trewick, S. C.; Henshaw, T. F.; Hausinger, R. P.; Lindahl, T.; Sedgwick, B. Oxidative Demethylation by Escherichia Coli Alkb Directly Reverts DNA Base Damage. *Nature* **2002,** *419*, 174-178.
(35) Falnes, P. O.; Johansen, R. F.; Seeberg, E. Alkb-Mediated Oxidative Demethylation Reverses DNA Damage in Escherichia Coli. *Nature* **2002,** *419* 178-182.
(36) Yi, C.; Jia, G.; Hou, G.; Dai, Q.; Zhang, W.; Zheng, G.; Jian, X.; Yang, C.-G.; Cui, Q.; He, C. Iron-Catalysed Oxidation Intermediates Captured in a DNA Repair Dioxygenase. *Nature* **2010,** *468*, 330-333.
(37) Wang, B.; Usharani, D.; Li, C.; Shaik, S. Theory Uncovers an Unusual Mechanism of DNA Repair of a Lesioned Adenine by Alkb Enzymes. *J. Am. Chem. Soc.* **2014,** *136*, 13895-13901.
(38) Cisneros, G. A. Dft Study of a Model System for the Dealkylation Step Catalyzed by Alkb. *Interdiscip. Sci.: Comput. Life Sci.* **2010,** *2*, 70-77.
(39) Cloos, P. A. C.; Christensen, J.; Agger, K.; Maiolica, A.; Rappsilber, J.; Antal, T.; Hansen, K. H.; Helin, K. The Putative Oncogene Gasc1 Demethylates Tri- and Dimethylated Lysine 9 on Histone H3. *Nature* **2006,** *442*, 307-311.
(40) Klose, R. J.; Yamane, K.; Bae, Y.; Zhang, D.; Erdjument-Bromage, H.; Tempst, P.; Wong, J.; Zhang, Y. The Transcriptional Repressor Jhdm3a Demethylates Trimethyl Histone H3 Lysine 9 and Lysine 36. *Nature* **2006,** *442*, 312-316.
(41) Tsukada, Y.; Fang, J.; Erdjument-Bromage, H.; Warren, M. E.; Borchers, C. H.; Tempst, P.; Zhang, Y. Histone Demethylation by a Family of Jmjc Domain-Containing Proteins. *Nature* **2006,** *439*, 811-816.
(42) Groves, J. T. Key Elements of the Chemistry of Cytochrome-P-450: The Oxygen Rebound Mechanism. *J. Chem. Educ.* **1985,** *62*, 928-931.
(43) Matthews, M. L.; Krest, C. M.; Barr, E. W.; Vaillancourt, F. H.; Walsh, C. T.; Green, M. T.; Krebs, C.; Bollinger, J. M. Substrate-Triggered Formation and Remarkable Stability of the C-H Bond-Cleaving Chloroferryl Intermediate in the Aliphatic Halogenase, Syrb2. *Biochemistry* **2009,** *48*, 4331-4343.
(44) Puri, M.; Biswas, A. N.; Fan, R.; Guo, Y.; Que, L. Modeling Non-Heme Iron Halogenases: High-Spin Oxoiron(Iv)-Halide Complexes That Halogenate C-H Bonds. *J. Am. Chem. Soc.* **2016,** *138*, 2484-2487.
(45) Yadav, V.; Rodriguez, R. J.; Siegler, M. A.; Goldberg, D. P. Determining the Inherent Selectivity for Carbon Radical Hydroxylation Versus Halogenation with Feiii(Oh)(X)

Complexes: Relevance to the Rebound Step in Non-Heme Iron Halogenases. *J. Am. Chem. Soc.* **2020,** *142*, 7259-7264.
(46) Kulik, H. J.; Drennan, C. L. Substrate Placement Influences Reactivity in Non-Heme Fe(Ii) Halogenases and Hydroxylases. *J. Biol. Chem.* **2013,** *288*, 11233-11241.
(47) Kulik, H. J.; Blasiak, L. C.; Marzari, N.; Drennan, C. L. First-Principles Study of Non-Heme Fe(Ii) Halogenase Syrb2 Reactivity. *J. Am. Chem. Soc.* **2010,** *131*, 14426-14433.
(48) Mehmood, R.; Qi, H. W.; Steeves, A. H.; Kulik, H. J. The Protein's Role in Substrate Positioning and Reactivity for Biosynthetic Enzyme Complexes: The Case of Syrb2/Syrb1. *ACS Catal.* **2019,** *9*, 4930-4943.
(49) Mehmood, R.; Vennelakanti, V.; Kulik, H. J. Spectroscopically Guided Simulations Reveal Distinct Strategies for Positioning Substrates to Achieve Selectivity in Nonheme Fe(Ii)/A-Ketoglutarate-Dependent Halogenases. *ACS Catal.* **2021,** *11*, 12394–12408.
(50) Kastner, D. W.; Nandy, A.; Mehmood, R.; Kulik, H. J. Mechanistic Insights into Substrate Positioning That Distinguish Non-Heme Fe(Ii)/A-Ketoglutarate-Dependent Halogenases and Hydroxylases. *ACS Catal.* **2023,** *13*, 2489-2501.
(51) Borowski, T.; Noack, H.; Radon, M.; Zych, K.; Siegbahn, P. E. M. Mechanism of Selective Halogenation by Syrb2: A Computational Study. *J. Am. Chem. Soc.* **2010,** *132*, 12887-12898.
(52) Huang, J.; Li, C.; Wang, B.; Sharon, D. A.; Wu, W.; Shaik, S. Selective Chlorination of Substrates by the Halogenase Syrb2 Is Controlled by the Protein According to a Combined Quantum Mechanics/Molecular Mechanics and Molecular Dynamics Study. *ACS Catal.* **2016,** *6*, 2694-2704.
(53) Timmins, A.; Fowler, N. J.; Warwicker, J.; Straganz, G. D.; de Visser, S. P. Does Substrate Positioning Affect the Selectivity and Reactivity in the Hectochlorin Biosynthesis Halogenase? *Front. Chem.* **2018,** *6*.
(54) Srnec, M.; Solomon, E. I. Frontier Molecular Orbital Contributions to Chlorination Versus Hydroxylation Selectivity in the Non-Heme Iron Halogenase Syrb2. *J. Am. Chem. Soc.* **2017,** *139*, 2396-2407.
(55) Pandian, S.; Vincent, M. A.; Hillier, I. H.; Burton, N. A. Why Does the Enzyme Syrb2 Chlorinate, but Does Not Hydroxylate, Saturated Hydrocarbons? A Density Functional Theory (Dft) Study. *Dalton T.* **2009**, 6201-6207.
(56) de Visser, S. P.; Latifi, R. Carbon Dioxide: A Waste Product in the Catalytic Cycle of A-Ketoglutarate Dependent Halogenases Prevents the Formation of Hydroxylated by-Products. *The Journal of Physical Chemistry B* **2009,** *113*, 12-14.
(57) Gérard, E. F.; Yadav, V.; Goldberg, D. P.; de Visser, S. P. What Drives Radical Halogenation Versus Hydroxylation in Mononuclear Nonheme Iron Complexes? A Combined Experimental and Computational Study. *J. Am. Chem. Soc.* **2022,** *144*, 10752-10767.
(58) Goudarzi, S.; Iyer, S. R.; Babicz, J. T.; Yan, J. J.; Peters, G. H. J.; Christensen, H. E. M.; Hedman, B.; Hodgson, K. O.; Solomon, E. I. Evaluation of a Concerted Vs. Sequential Oxygen Activation Mechanism in A-Ketoglutarate-Dependent Nonheme Ferrous Enzymes. *Proc. Natl. Acad. Sci. U. S. A.* **2020,** *117*, 5152-5159.
(59) Solomon, E. I.; DeWeese, D. E.; Babicz, J. T. Mechanisms of O2 Activation by Mononuclear Non-Heme Iron Enzymes. *Biochemistry* **2021,** *60*, 3497-3506.
(60) Solomon, E. I.; Goudarzi, S.; Sutherlin, K. D. O2 Activation by Non-Heme Iron Enzymes. *Biochemistry* **2016,** *55*, 6363-6374.

(61) Alvarez-Barcia, S.; Kästner, J. Atom Tunneling in the Hydroxylation Process of Taurine/A-Ketoglutarate Dioxygenase Identified by Quantum Mechanics/Molecular Mechanics Simulations. *The Journal of Physical Chemistry B* **2017,** *121*, 5347-5354.
(62) Mandal, D.; Mallick, D.; Shaik, S. Kinetic Isotope Effect Determination Probes the Spin of the Transition State, Its Stereochemistry, and Its Ligand Sphere in Hydrogen Abstraction Reactions of Oxoiron(Iv) Complexes. *Acc. Chem. Res.* **2018,** *51*, 107-117.
(63) Sastri, C. V.; Lee, J.; Oh, K.; Lee, Y. J.; Lee, J.; Jackson, T. A.; Ray, K.; Hirao, H.; Shin, W.; Halfen, J. A.; Kim, J.; Que, L.; Shaik, S.; Nam, W. Axial Ligand Tuning of a Nonheme Iron(Iv)-Oxo Unit for Hydrogen Atom Abstraction. *Proc. Natl. Acad. Sci. U. S. A.* **2007,** *104*, 19181-19186.
(64) Gibbons, H. S.; Lin, S.; Cotter, R. J.; Raetz, C. R. H. Oxygen Requirement for the Niosynthesis of the S-2-Hydroxymyristate Moiety in Salmonella Typhimurium Lipid a -: Function of Lpxo, a New Fe2+/A-Ketoglutarate-Dependent Dioxygenase Homologue. *J. Biol. Chem.* **2000,** *275*, 32940-32949.
(65) Croes, K.; Foulon, V.; Casteels, M.; Van Veldhoven, P. P.; Mannaerts, G. P. Phytanoyl-Coa Hydroxylase: Recognition of 3-Methyl-Branched Acyl-Coas and Requirement for Gtp or Atp and Mg2+ in Addition to Its Known Hydroxylation Cofactors. *J. Lipid Res.* **2000,** *41*, 629-636.
(66) Choroba, O. W.; Williams, D. H.; Spencer, J. B. Biosynthesis of the Vancomycin Group of Antibiotics: Involvement of an Unusual Dioxygenase in the Pathway to (S)-4-Hydroxyphenylglycine. *J. Am. Chem. Soc.* **2000,** *122*, 5389-5390.
(67) Higgins, L. J.; Yan, F.; Liu, P.; Liu, H.-w.; Drennan, C. L. Structural Insight into Antibiotic Fosfomycin Biosynthesis by a Mononuclear Iron Enzyme. *Nature* **2005,** *437*, 838-844.
(68) Bodner, M. J.; Phelan, R. M.; Freeman, M. F.; Li, R.; Townsend, C. A. Non-Heme Iron Oxygenases Generate Natural Structural Diversity in Carbapenem Antibiotics. *J. Am. Chem. Soc.* **2010,** *132*, 12-13.
(69) Galonic, D. P.; Barr, E. W.; Walsh, C. T.; Bollinger, J. M.; Krebs, C. Two Interconverting Fe((Iv)) Intermediates in Aliphatic Chlorination by the Halogenase Cytc3. *Nat. Chem. Biol.* **2007,** *3*, 113-116.
(70) Mitchell, A. J.; Dunham, N. P.; Bergman, J. A.; Wang, B.; Zhu, Q.; Chang, W.; Liu, X.; Boal, A. K. Structure-Guided Reprogramming of a Hydroxylase to Halogenate Its Small Molecule Substrate. *Biochemistry* **2017,** *56*, 441-444.
(71) Koehntop, K. D.; Emerson, J. P.; Que, L. The 2-His-1-Carboxylate Facial Triad: A Versatile Platform for Dioxygen Activation by Mononuclear Non-Heme Iron (Ii) Enzymes. *J. Biol. Inorg. Chem.* **2005,** *10*, 87-93.
(72) Que Jr, L. One Motif—Many Different Reactions. *Nat. Struct. Mol. Biol.* **2000,** *7*, 182.
(73) Martinie, R. J.; Pollock, C. J.; Matthews, M. L.; Bollinger, J. M.; Krebs, C.; Silakov, A. Vanadyl as a Stable Structural Mimic of Reactive Ferryl Intermediates in Mononuclear Nonheme-Iron Enzymes. *Inorg. Chem.* **2017,** *56*, 13382-13389.
(74) Bollinger Jr., J. M.; Krebs, C. Stalking Intermediates in Oxygen Activation by Iron Enzymes: Motivation and Method. *J. Inorg. Biochem.* **2006,** *100*, 586-605.
(75) Price, J. C.; Barr, E. W.; Tirupati, B.; Bollinger, J. M.; Krebs, C. The First Direct Characterization of a High-Valent Iron Intermediate in the Reaction of an Alpha-Ketoglutarate-Dependent Dioxygenase: A High-Spin Fe(Iv) Complex in Taurine/Alpha-Ketoglutarate Dioxygenase (Taud) from Escherichia Coli. *Biochemistry* **2003,** *42*, 7497-7508.

(76) Wong, S. D.; Srnec, M.; Matthews, M. L.; Liu, L. V.; Kwak, Y.; Park, K.; Bell, C. B.; Alp, E. E.; Zhao, J.; Yoda, Y.; Kitao, S.; Seto, M.; Krebs, C.; Bollinger, J. M.; Solomon, E. I. Elucidation of the Fe(Iv)=O Intermediate in the Catalytic Cycle of the Halogenase Syrb2. *Nature* **2013,** *499*, 320-323.
(77) Martinie, R. J.; Livada, J.; Chang, W.-c.; Green, M. T.; Krebs, C.; Bollinger, J. M.; Silakov, A. Experimental Correlation of Substrate Position with Reaction Outcome in the Aliphatic Halogenase, Syrb2. *J. Am. Chem. Soc.* **2015,** *137*, 6912-6919.
(78) Rohde, J.-U.; In, J.-H.; Lim, M. H.; Brennessel, W. W.; Bukowski, M. R.; Stubna, A.; Münck, E.; Nam, W.; Que, L. Crystallographic and Spectroscopic Characterization of a Nonheme Fe(Iv)=O Complex. *Science* **2003,** *299*, 1037-1039.
(79) Klinker, E. J.; Kaizer, J.; Brennessel, W. W.; Woodrum, N. L.; Cramer, C. J.; Que, L. Structures of Nonheme Oxoiron(Iv) Complexes from X-Ray Crystallography, Nmr Spectroscopy, and Dft Calculations. *Angew. Chem., Int. Ed.* **2005,** *44*, 3690-3694.
(80) Rohde, J.-U.; Torelli, S.; Shan, X.; Lim, M. H.; Klinker, E. J.; Kaizer, J.; Chen, K.; Nam, W.; Que, L. Structural Insights into Nonheme Alkylperoxoiron(Iii) and Oxoiron(Iv) Intermediates by X-Ray Absorption Spectroscopy. *J. Am. Chem. Soc.* **2004,** *126*, 16750-16761.
(81) Pestovsky, O.; Stoian, S.; Bominaar, E. L.; Shan, X.; Münck, E.; Que, L.; Bakac, A. Aqueous Feiv=O: Spectroscopic Identification and Oxo-Group Exchange. *Angew. Chem., Int. Ed.* **2005,** *44*, 6871-6874.
(82) Grapperhaus, C. A.; Mienert, B.; Bill, E.; Weyhermüller, T.; Wieghardt, K. Mononuclear (Nitrido)Iron(V) and (Oxo)Iron(Iv) Complexes Via Photolysis of [(Cyclam-Acetato)Feiii(N3)]+ and Ozonolysis of [(Cyclam-Acetato)Feiii(O3scf3)]+ in Water/Acetone Mixtures. *Inorg. Chem.* **2000,** *39*, 5306-5317.
(83) Ehudin, M. A.; Gee, L. B.; Sabuncu, S.; Braun, A.; Moenne-Loccoz, P.; Hedman, B.; Hodgson, K. O.; Solomon, E. I.; Karlin, K. D. Tuning the Geometric and Electronic Structure of Synthetic High-Valent Heme Iron(Iv)-Oxo Models in the Presence of a Lewis Acid and Various Axial Ligands. *J. Am. Chem. Soc.* **2019,** *141*, 5942-5960.
(84) Davis, K. M.; Altmyer, M.; Martinie, R. J.; Schaperdoth, I.; Krebs, C.; Bollinger, J. M.; Boal, A. K. Structure of a Ferryl Mimic in the Archetypal Iron(Ii)- and 2-(Oxo)-Glutarate-Dependent Dioxygenase, Taud. *Biochemistry* **2019,** *58*, 4218-4223.
(85) Dunham, N. P.; Chang, W.-c.; Mitchell, A. J.; Martinie, R. J.; Zhang, B.; Bergman, J. A.; Rajakovich, L. J.; Wang, B.; Silakov, A.; Krebs, C.; Boal, A. K.; Bollinger, J. M. Two Distinct Mechanisms for C-C Desaturation by Iron(Ii)- and 2-(Oxo)Glutarate-Dependent Oxygenases: Importance of Alpha-Heteroatom Assistance. *J. Am. Chem. Soc.* **2018,** *140*, 7116-7126.
(86) Chekan, J. R.; Ongpipattanakul, C.; Wright, T. R.; Zhang, B.; Bollinger, J. M.; Rajakovich, L. J.; Krebs, C.; Cicchillo, R. M.; Nair, S. K. Molecular Basis for Enantioselective Herbicide Degradation Imparted by Aryloxyalkanoate Dioxygenases in Transgenic Plants. *Proc. Natl. Acad. Sci. U. S. A.* **2019,** *116*, 13299-13304.
(87) Mitchell, A. J.; Dunham, N. P.; Martinie, R. J.; Bergman, J. A.; Pollock, C. J.; Hu, K.; Allen, B. D.; Chang, W.-c.; Silakov, A.; Bollinger, J. M.; Krebs, C.; Boal, A. K. Visualizing the Reaction Cycle in an Iron(Ii)- and 2-(Oxo)-Glutarate-Dependent Hydroxylase. *J. Am. Chem. Soc.* **2017,** *139*, 13830-13836.

(88) Vennelakanti, V.; Mehmood, R.; Kulik, H. J. Are Vanadium Intermediates Suitable Mimics in Non-Heme Iron Enzymes? An Electronic Structure Analysis. *ACS Catal.* **2022,** *12*, 5489-5501.
(89) Hirao, H.; Kumar, D.; Que, L., Jr.; Shaik, S. Two-State Reactivity in Alkane Hydroxylation by Non-Heme Iron-Oxo Complexes. *J. Am. Chem. Soc.* **2006,** *128*, 8590-8606.
(90) Shaik, S.; Danovich, D.; Fiedler, A.; Schroder, D.; Schwarz, H. 2-State Reactivity in Organometallic Gas-Phase Ion Chemistry. *Helv Chim Acta* **1995,** *78*, 1393-1407.
(91) Schroder, D.; Shaik, S.; Schwarz, H. Two-State Reactivity as a New Concept in Organometallic Chemistry. *Acc. Chem. Res.* **2000,** *33*, 139-145.
(92) Abram, S.-L.; Monte-Perez, I.; Pfaff, F. F.; Farquhar, E. R.; Ray, K. Evidence of Two-State Reactivity in Alkane Hydroxylation by Lewis-Acid Bound Copper-Nitrene Complexes. *Chemical Communications* **2014,** *50*, 9852-9854.
(93) Rohde, J.-U.; Que, L. Axial Coordination of Carboxylate Activates the Non-Heme Fe-Iv=O Unit. *Angew. Chem., Int. Ed.* **2005,** *44*, 2255-2258.
(94) Bukowski, M. R.; Koehntop, K. D.; Stubna, A.; Bominaar, E. L.; Halfen, J. A.; Munck, E.; Nam, W.; Que, L. A Thiolate-Ligated Nonheme Oxoiron(Iv) Complex Relevant to Cytochrome P450. *Science* **2005,** *310*, 1000-1002.
(95) Decker, A.; Rohde, J.-U.; Que, L.; Solomon, E. I. Spectroscopic and Quantum Chemical Characterization of the Electronic Structure and Bonding in a Non-Heme Fe-Iv=O Complex. *J. Am. Chem. Soc.* **2004,** *126*, 5378-5379.
(96) Decker, A.; Solomon, E. I. Comparison of Fe-Iv=O Heme and Non-Heme Species: Electronic Structures, Bonding, and Reactivities. *Angew. Chem., Int. Ed.* **2005,** *44*, 2252-2255.
(97) Schoneboom, J. C.; Neese, F.; Thiel, W. Toward Identification of the Compound I Reactive Intermediate in Cytochrome P450 Chemistry: A Qm/Mm Study of Its Epr and Mossbauer Parameters. *J. Am. Chem. Soc.* **2005,** *127*, 5840-5853.
(98) Srnec, M.; Wong, S. D.; Matthews, M. L.; Krebs, C.; Bollinger, J. M.; Solomon, E. I. Electronic Structure of the Ferryl Intermediate in the A-Ketoglutarate Dependent Non-Heme Iron Halogenase Syrb2: Contributions to H Atom Abstraction Reactivity. *J. Am. Chem. Soc.* **2016,** *138*, 5110-5122.
(99) Fujimori, D. G.; Barr, E. W.; Matthews, M. L.; Koch, G. M.; Yonce, J. R.; Walsh, C. T.; Bollinger, J. M.; Krebs, C.; Riggs-Gelasco, P. J. Spectroscopic Evidence for a High-Spin Br-Fe(Iv)-Oxo Intermediate in the Alpha-Ketoglutarate-Dependent Halogenase Cytc3 from Streptomyces. *J. Am. Chem. Soc.* **2007,** *129*, 13408-13409.
(100) Ballhausen, C. J.; Gray, H. B. The Electronic Structure of the Vanadyl Ion. *Inorg. Chem.* **1962,** *1*, 111–122.
(101) Dunham, N. P.; Mitchell, A. J.; Pantoja, J. M. D. R.; Krebs, C.; Bollinger, J. M.; Boal, A. K. Alpha-Amine Desaturation of D-Arginine by the Iron(Ii)- and 2-(Oxo)Glutarate-Dependent L-Arginine 3-Hydroxylase, Vioc. *Biochemistry* **2018,** *57*, 6479-6488.
(102) Yin, X.; Zabriskie, T. M. Vioc Is a Non-Heme Iron, Alpha-Ketoglutarate-Dependent Oxygenase That Catalyzes the Formation of 3s-Hydroxy-L-Arginine During Viomycin Biosynthesis. *ChemBioChem* **2004,** *5*, 1274-1277.
(103) Hanwell, M. D.; Curtis, D. E.; Lonie, D. C.; Vandermeersch, T.; Zurek, E.; Hutchison, G. R. Avogadro: An Advanced Semantic Chemical Editor, Visualization, and Analysis Platform. *J. Cheminf.* **2012,** *4*, 17.

(104) Rappe, A. K.; Casewit, C. J.; Colwell, K. S.; Goddard, W. A. I.; Skiff, W. M. Uff, a Full Periodic-Table Force-Field for Molecular Mechanics and Molecular-Dynamics Simulations. *J. Am. Chem. Soc.* **1992,** *114*, 10024-10035.
(105) Ioannidis, E. I.; Gani, T. Z. H.; Kulik, H. J. Molsimplify: A Toolkit for Automating Discovery in Inorganic Chemistry. *J. Comput. Chem.* **2016,** *37*, 2106-2117.
(106) O'Boyle, N. M.; Morley, C.; Hutchison, G. R. Pybel: A Python Wrapper for the Openbabel Cheminformatics Toolkit. *Chem. Cent. J.* **2008,** *2*, 5.
(107) O'Boyle, N. M.; Banck, M.; James, C. A.; Morley, C.; Vandermeersch, T.; Hutchison, G. R. Open Babel: An Open Chemical Toolbox. *J. Cheminf.* **2011,** *3*, 33.
(108) Neese, F. Software Update: The Orca Program System, Version 4.0. *Wiley Interdiscip. Rev.: Comput. Mol. Sci.* **2018,** *8*, e1327.
(109) Adamo, C.; Barone, V. Toward Reliable Density Functional Methods without Adjustable Parameters: The Pbe0 Model. *J. Chem. Phys.* **1999,** *110*, 6158-6170.
(110) Weigend, F.; Ahlrichs, R. Balanced Basis Sets of Split Valence, Triple Zeta Valence and Quadruple Zeta Valence Quality for H to Rn: Design and Assessment of Accuracy. *Phys. Chem. Chem. Phys.* **2005,** *7*, 3297-3305.
(111) Grimme, S.; Antony, J.; Ehrlich, S.; Krieg, H. A Consistent and Accurate Ab Initio Parametrization of Density Functional Dispersion Correction (Dft-D) for the 94 Elements H-Pu. *J. Chem. Phys.* **2010,** *132*, 154104.
(112) Grimme, S.; Ehrlich, S.; Goerigk, L. Effect of the Damping Function in Dispersion Corrected Density Functional Theory. *J. Comput. Chem.* **2011,** *32*, 1456-1465.
(113) Barone, V.; Cossi, M. Quantum Calculation of Molecular Energies and Energy Gradients in Solution by a Conductor Solvent Model. *J. Phys. Chem. A* **1998,** *102*, 1995-2001.
(114) Lu, T.; Chen, F. Multiwfn: A Multifunctional Wavefunction Analyzer. *J. Comput. Chem.* **2012,** *33*, 580-592.
(115) Clifton, I. J.; McDonough, M. A.; Ehrismann, D.; Kershaw, N. J.; Granatino, N.; Schofield, C. J. Structural Studies on 2-Oxoglutarate Oxygenases and Related Double-Stranded Beta-Helix Fold Proteins. *J. Inorg. Biochem.* **2006,** *100*, 644-669.
(116) Casey, T. M.; Grzyska, P. K.; Hausinger, R. P.; McCracken, J. Measuring the Orientation of Taurine in the Active Site of the Nonheme Fe(Ii)/Alpha-Ketoglutarate-Dependent Taurine Hydroxylase (Taud) Using Electron Spin Echo Envelope Modulation (Eseem) Spectroscopy. *The Journal of Physical Chemistry B* **2013,** *117*, 10384-10394.
(117) Pavel, E. G.; Zhou, J.; Busby, R. W.; Gunsior, M.; Townsend, C. A.; Solomon, E. I. Circular Dichroism and Magnetic Circular Dichroism Spectroscopic Studies of the Non-Heme Ferrous Active Site in Clavaminate Synthase and Its Interaction with Alpha-Ketoglutarate Cosubstrate. *J. Am. Chem. Soc.* **1998,** *120*, 743-753.
(118) Ryle, M. J.; Padmakumar, R.; Hausinger, R. P. Stopped-Flow Kinetic Analysis of Escherichia Coli Taurine/Alpha-Ketoglutarate Dioxygenase: Interactions with Alpha-Ketoglutarate, Taurine, and Oxygen. *Biochemistry* **1999,** *38*, 15278-15286.
(119) Elkins, J. M.; Ryle, M. J.; Clifton, I. J.; Hotopp, J. C. D.; Lloyd, J. S.; Burzlaff, N. I.; Baldwin, J. E.; Hausinger, R. P.; Roach, P. L. X-Ray Crystal Structure of Escherichia Coli Taurine/Alpha-Ketoglutarate Dioxygenase Complexed to Ferrous Iron and Substrates. *Biochemistry* **2002,** *41*, 5185-5192.
(120) de Visser, S. P. Elucidating Enzyme Mechanism and Intrinsic Chemical Properties of Short-Lived Intermediates in the Catalytic Cycles of Cysteine Dioxygenase and Taurine/Alpha-Ketoglutarate Dioxygenase. *Coord. Chem. Rev.* **2009,** *253*, 754-768.

(121) de Visser, S. P.; Latifi, R.; Tahsini, L.; Nam, W. The Axial Ligand Effect on Aliphatic and Aromatic Hydroxylation by Non-Heme Iron(Iv)-Oxo Biomimetic Complexes. *Chem. - Asian J.* **2011,** *6*, 493-504.
(122) Purpero, V.; Moran, G. R. The Diverse and Pervasive Chemistries of the Alpha-Keto Acid Dependent Enzymes. *J. Biol. Inorg. Chem.* **2007,** *12*, 587-601.
(123) Bollinger, J. M. J.; Price, J. C.; Hoffart, L. M.; Barr, E. W.; Krebs, C. Mechanism of Taurine: Alpha-Ketoglutarate Dioxygenase (Taud) from Escherichia Coli. *Eur. J. Inorg. Chem.* **2005,** *2005*, 4245-4254.
(124) Timmins, A.; de Visser, S. P. A Comparative Review on the Catalytic Mechanism of Nonheme Iron Hydroxylases and Halogenases. *Catalysts* **2018,** *8*, 314.
(125) Muthukumaran, R. B.; Grzyska, P. K.; Hausinger, R. P.; McCracken, J. Probing the Iron-Substrate Orientation for Taurine/Alpha-Ketoglutarate Dioxygenase Using Deuterium Electron Spin Echo Envelope Modulation Spectroscopy. *Biochemistry* **2007,** *46*, 5951-5959.
(126) Sinnecker, S.; Svensen, N.; Barr, E. W.; Ye, S.; Bollinger, J. M.; Neese, F.; Krebs, C. Spectroscopic and Computational Evaluation of the Structure of the High-Spin Fe(Iv)-Oxo Intermediates in Taurine: Alpha-Ketoglutarate Dioxygenase from Escherichia Coli and Its His99ala Ligand Variant. *J. Am. Chem. Soc.* **2007,** *129*, 6168-6179.
(127) Neidig, M. L.; Decker, A.; Choroba, O. W.; Huang, F.; Kavana, M.; Moran, G. R.; Spencer, J. B.; Solomon, E. I. Spectroscopic and Electronic Structure Studies of Aromatic Electrophilic Attack and Hydrogen-Atom Abstraction by Non-Heme Iron Enzymes. *Proc. Natl. Acad. Sci. U. S. A.* **2006,** *103*, 12966-12973.

TOC Graphic